Live Cell Imaging and Real-Time Monitoring Nucleolus Morphology and Mitophagy with a Red Fluorescent and Photostable rRNA-Specific Probe in Human Cancer Cells

Jun-Ren Luo [§,a], Wei Long [§,*,b,c], Ze-Xin Chen [§,a], Shi-Min Wang [a], Yao-Xun Zeng [c], Yu-Jing Lu [*,a], Bo-Xin Zheng [b], Meng-Ting She [c] and Wing-Leung Wong [*,b,c]

[a] School of Biomedical and Pharmaceutical Sciences, Guangdong University of Technology, Guangzhou 510006, P. R. China.

[b] State Key Laboratory of Chemical Biology and Drug Discovery, Department of Applied Biology and Chemical Technology, The Hong Kong Polytechnic University, Hung Hom, Kowloon, Hong Kong SAR 999077, China.

[c] The Hong Kong Polytechnic University Shenzhen Research Institute, Shenzhen 518057, P. R. China.

§ These authors contributed equally to this work.

* Corresponding author.

E-mail (W. Long): wei-abct.long@polyu.edu.hk

E-mail (Y.-J. Lu): luyj@gdut.edu.cn

E-mail (W.-L. Wong): wing.leung.wong@polyu.edu.hk

ABSTRACT

rRNAs are prevalent in living organisms. They are produced in nucleolus and mitochondria, and play essential cellular functions. In addition to the primary biofunctions in protein synthesis, rRNAs have been recognized as the emerging signaling molecule and drug target for studies on nucleolus morphology, mitochondrial autophagy and tumor cell malignancy. Currently, only few rRNA-selective probes have been developed and most of them encounter the drawbacks of low water solubility, poor nuclear membrane permeability, short emission wavelength, low stability against photobleaching and high cytotoxicity. These unfavorable properties of rRNA probes limit the potential applications. In the present study, we reported a new rRNA-selective and near-infrared fluorescent turn-on probe, **4MPS-TO**, capable of tracking rRNA in live human cancer cells. The real-time monitoring performance in nucleolus morphology and mitochondrial autophagy is demonstrated in live HeLa cells. The probe shows great application potential for being used as a rRNA-selective, sensitive and photostable imaging tool in chemical biology study and drug screening.

KEYWORDS: molecular rRNA sensor, red fluorescent probe, nucleolus morphology, autophagy, live cell imaging

Ribonucleic acids (RNAs) are critically important biomolecules because they are responsible for gene coding, transcriptional regulation, protein expression and catalyzing biological reactions in live cells.[1,2] RNAs are a big family and primarily comprise non-coding RNA, messenger RNA (mRNA), transfer RNA (tRNA) and ribosomal RNA (rRNA). Among the RNA family, rRNAs are the most prevalent in living organisms and produced in nucleolus and mitochondria.[3,4] In all living organisms, rRNA and several ribosomal proteins are an integral part of ribosomes, which are essential machines for protein synthesis.[5,6] In recent years, to understand the relationship between nucleolus morphology and tumor cell malignancy is a hot research topic,[7-9] in which the rRNA has been known serving as substantial signaling molecules.[10] Moreover, a specific and nongenotoxic inhibition of rRNA transcription could cause selective damage to neoplastic cells.[11-13] Furthermore, understanding the correlation between ribosome biogenesis and cell proliferation, and the effect of ribosome biogenesis inhibitors on the selective cytotoxicity of cancer cells can provide critical information on cancer biology.[14,15] Therefore, rRNA is a very important cellular target for investigation. The cell-membrane and nuclear-membrane permeable, sensitive, selective, photostable and nontoxic small-sized fluorescent probes are the indispensable chemical tool allowing biological and biochemical investigations in live cells and/or *in vivo* conditions. The intricate three-dimensional structure of rRNA,[16] compared to DNA structures, is more complicated and thus it poses a formidable challenge for the design of fluorescent probes targeting rRNA with high specificity, particularly in live cell and/or *in vivo* imaging. Currently, SYTO RNA-Select is the only commercially available dye for RNA imaging; however, its molecular structure is not known, its excitation and emission are approximately 490/530 nm, and the photostability is low under cellular conditions.[17] More importantly, with respect to the most recent reviews on the RNA-selective probes

development,[18,19] only few probes have been developed at present and they commonly encounter some drawbacks of low water solubility, poor nuclear membrane permeability, short emission wavelength, low stability against photobleaching, and relatively high cytotoxicity. These adverse properties of most reported rRNA probes limit their potential applications in real-time live cell imaging and biomedical and clinical areas. To best of our knowledge, E36,[20] luminescent alkynylplatinum(II) derivative 1,[21] naphthalimide derivative 1,[22] CP,[23] Styryl-TO,[17] and PI2[24] are the only known rRNA-targeting fluorescent turn-on probes being demonstrated in live cells currently. Therefore, the novel molecular design to further advance rRNA probes for different applications is needed, particularly the cell membrane and nuclear membrane permeable rRNA-specific red emission probes.

Thiazole orange (TO), an optically excellent non-specific nucleic acid dye, has been subjected to quite a lot of modifications in recent years,[25] such as its derivatives TOTO-1 and YOYO-1. These ligands are currently one of the most sensitive and commercially available probes for sensing and imaging of nucleic acids.[26,27] TO can be also tailored to be target- and/or organelle-specific, such as the G-quadruplex-DNA-selective probe (TO-derivative 3) and the mitochondria-selective probe (TOVJ).[28,29] We have previously developed a green fluorescent probe, Styryl-TO,[17] also modified from TO scaffold for rRNA sensing and real-time imaging in live human cancer cells. This rRNA-selective probe shows excellent sensitivity and selectivity, low toxicity, and high stability against photobleaching. Nonetheless, to further shift the excitation and emission wavelength of rRNA probes to a longer wavelength close to the near infrared (NIR) region for real-time live cell imaging and/or bioimaging applications remains a challenge.

In this study, a new red fluorescent rRNA-targeting probe, **4MPS-TO**, was developed based on a TO scaffold modified with a rigid aromatic styryl moiety that was functionalized with a polar *N*-

methylpiperazinyl terminal group (Scheme S1). **4MPS-TO** upon binding to rRNA in a pH 7.4 buffer shows a rapid and markedly enhanced deep red fluorescent signal. More importantly, it has good water solubility and strong anti-photobleaching performance, which is much better than the commercial and reported RNA probes. The working concentration of **4MPS-TO** to image cellular rRNA in living cells is low (≤ 2.5 μM). The ligand enters live cells in about 20 min allowing real-time tracing dynamic activity of rRNAs in both nucleolus regions and mitochondria in live human HeLa cells.

EXPERIMENTAL SECTION

Detailed information of experimental methods and bioassay conditions is given in Supporting Information. The materials and experimental procedures for synthesis and characterization, and cell imaging were briefly described as follows:

Materials and Reagents. All materials and reagents were obtained from established commercial suppliers and used without further purification.

Synthesis of 4MPS-TO. Compound **a** was obtained by the reaction using 2-chloro-1,4-dimethylquinolin-1-ium iodide (0.638 g, 2.0 mmol) and 2,3-dimethylbenzo[d]thiazol-3-ium iodide (0.582 g, 2.0 mmol) in methanol at 40 °C for 12 h. Further reaction of **a** (0.446 g, 1.0 mmol) with 4-(4-methylpiperazin-1-yl)benzaldehyde (0.306 g, 1.5 mmol) and 4-methylpiperidine (100 μL) in acetonitrile (10 mL) was conducted in reflux condition (about 110 °C) for 3 h to afford the target compound **4MPS-TO** with good isolated yield (82.7%) (Scheme S1). **4MPS-TO** was purified by flash silica gel column chromatography and was confirmed with ^{1}H NMR, ^{13}C NMR, and HRMS (Figure S15). The purity of the compound was determined by HPLC is higher than 95%.

Spectral Analysis. UV-Vis and fluorescence spectra were obtained using a Lambda 25 spectrophotometer (Perkin Elmer) and in an LS-45 fluorescence spectrometer (Perkin Elmer). The cuvette had a slit width of 1 mm and an optical diameter of 10 mm. CD spectra were measured using a chromatograph spectrophotometer (Applied Photophysics). Tris-HCl buffer (10 mM containing 60 mM KCl, pH = 7.4) was used to prepare a 100 μg/ml solution of rRNA, tRNA Ds26. Spectral data were recorded in the wavelength range 220–700 nm with a bandwidth of 2 nm, a step size of 1 nm and a point count of 0.1 s/point using a quartz cuvette with a path length of 1 mm. The CD spectral data obtained were averaged over three scans. The data were then analyzed using Origin 2018.

^{1}H NMR titration study. The rRNA solution (10 mg/mL) was prepared in phosphate buffer (25 mM monopotassium phosphate, 10% D_2O-d_2, 70 mM KCl, pH = 7.4) and was kept at -20 °C. During the measurement process, 1.59 mg of **4MPS-TO** was dissolved in DMSO-d_6, and then the rRNA solution (10 mg/mL) was added to the **4MPS-TO** solution for nuclear magnetic resonance analysis. rRNAs were added three times, each with a volume of 20 μL. The experiments were performed at 25 °C on a 600 MHz spectrometer (Bruker).

Cellular Imaging Studies. HeLa cells (CRM-CCL-2) were used for the study. The cells were thawed from liquid nitrogen storage and resuspended in DMEM medium supplemented with 10% fetal bovine serum (FBS) and 1% antifungal antibiotic. They were then cultured in an incubator at 37 °C with 5% CO_2. The cells were cultured in confocal dishes until they reached the logarithmic phase of growth. Different concentrations of **4MPS-TO**, nucleus probe Hoechst 33342, commercial organelle probes, RNA probes such as Stryl-TO, nuclease (DNase I and RNase A), G4-DNA inhibitor (Braco19), RNA synthesis inhibitor (CX5461 and actinomycin D), and oxidative stress inducer (H_2O_2) were used for

imaging and analysis, and the above analyses were performed on a Zeiss LSM800 confocal laser scanning microscope. In addition, fluorescence lifetime imaging microscopy (FLIM) imaging of **4MPS-TO** was performed using Leica SP8 FALCON. Fluorescence intensity, colocalization, nucleolus and nucleus area were quantified by image J.

RESULTS AND DISCUSSION

Spectral Properties of the Small Molecule Fluorescent Probe. The new rRNA probe, **4MPS-TO**, is designed to bear a typical intramolecular charge transfer (ICT) molecular structure of D-π-A-π-D,[30] in which (4-methylpiperazin-1-yl)styryl and benzothiazole moieties act as electron donors and the quinoline moiety acts as an electron acceptor (Scheme S1). The water solubility of the ligand determined is 118.3 μg/mL (187.1 μM, Figure S1A). The ligand has an intensive absorption in the region of 400-600 nm ($\varepsilon_{520\ nm}$ = 21360 $M^{-1}\cdot cm^{-1}$ in a pH 7.4 Tris-HCl solution containing rRNA, Figure S1B). It shows only weak emission in solution due to the non-radiative decay causing by free intramolecular rotations. The fluorescence of **4MPS-TO** in viscous glycerol medium was enhanced up to 80-fold due to the inhibition of intramolecular rotation (Figure S1C). UV-Vis titrations (Figure S1D) demonstrated that the characteristic absorption peak of **4MPS-TO** was at 464 nm. As the concentration of rRNA increased, the characteristic absorption peak of **4MPS-TO** increased, resulting in an obvious red-shift phenomenon. Additionally, a new characteristic absorption peak was formed at 520 nm, indicating a binding effect between **4MPS-TO** and rRNA. To verify the selectivity of **4MPS-TO** targeting rRNA, other nucleic acids, amino acids and protein substrates were also examined in fluorescence titrations (Figure 1A and Figure S2). The results show that rRNA enhances the fluorescence signal at least 4-fold higher than other

types of RNAs, 11-fold higher than the double-stranded DNA, at least 27-fold higher than the single-stranded DNA, and at least 2.3-fold higher than G4-DNAs tested. More importantly, there is only a 2-fold increase in fluorescence signals between **4MPS-TO** and amino acids, BSA or nucleolin, indicating that it may preclude the influence of these substances in the cellular environment, especially nucleolin proteins that are enriched in the nucleolus of cells. These results support that **4MPS-TO** is highly selective in imaging of rRNAs in the nucleolus. As shown in Figure 1B, the ligand responds to rRNA and emits red fluorescence (λ_{ex} = 520 nm; λ_{em} = 620 nm) in a concentration-dependent manner. An enhanced intensity up to 168-fold is observed. The absolute fluorescence quantum yield of **4MPS-TO** upon interacting with rRNA is increased from 0.38 to 4.83 (Figure S3 and Figure S4). Naked-eye visualization of **4MPS-TO**-rRNA interaction is also achievable under an UV-lamp irradiation (Figure 1D).

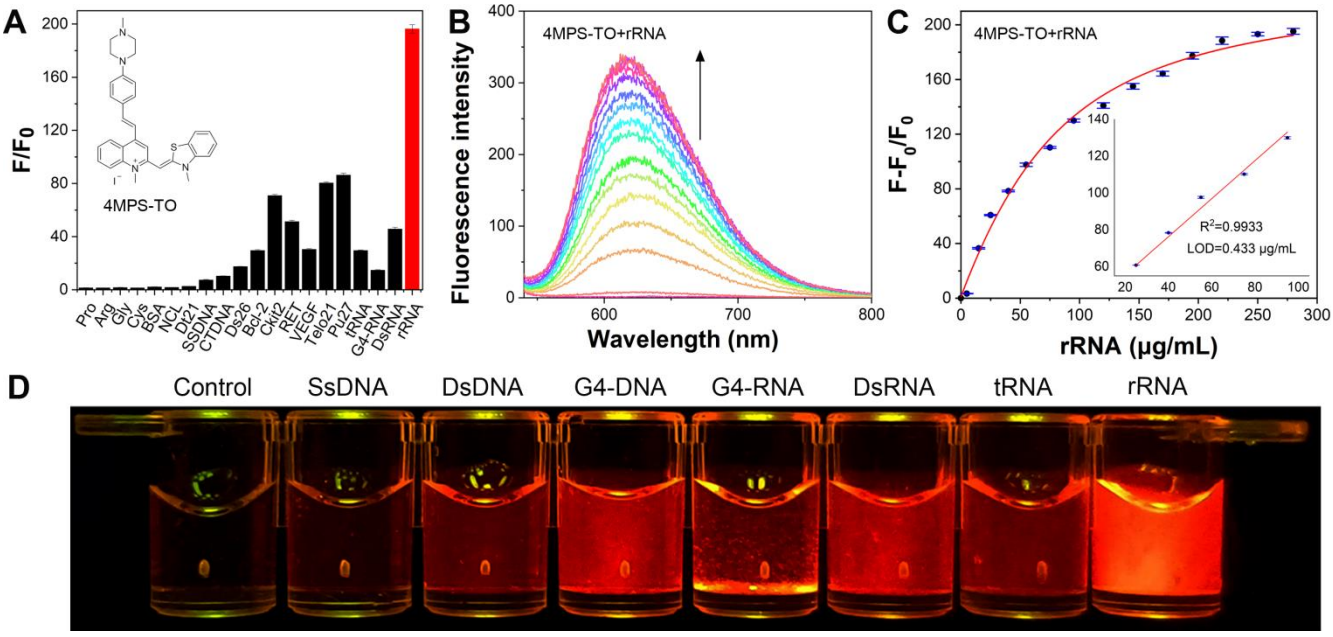

Figure 1. (A) Selectivity screening based on induced fluorescence responses of **4MPS-TO** (2.5 μM) upon binding with various substrates (280 μg/mL) in a Tris-HCl buffer (10 mM, pH 7.4, containing 60 mM KCl). F_0 represents the fluorescence intensity without nucleic acids and F represents the fluorescence intensity after adding nucleic acids. (B) Fluorescence titration spectra of **4MPS-TO** (2.5 μM) with rRNA

(280 μg/mL) in a Tris-HCl buffer (10 mM, pH 7.4, containing 60 mM KCl). (C) Fitted curve and linear relationship of **4MPS-TO** with rRNA (280 μg/mL). (D) Different nucleic acids (280 μg/mL) were separately added to **4MPS-TO** (2.5 μM) and incubated for 1 h (Tris-HCl =10 mM, pH 7.4, containing 60 mM KCl). The fluorescence signals were subsequently observed under a laboratory UV light (wavelength 302 nm).

Table 1. Equilibrium binding constants (K_{eq}) for the interaction of ligand and substrates at 25 °C. [a]

Substrates	Structure/origin	K_{eq} ($\times 10^5$ M^{-1})
Pro	Amino acid	n.d.
Arg	Amino acid	n.d.
Gly	Amino acid	n.d.
Cys	Amino acid	n.d.
BSA	Protein	n.d.
NCL	Protein	n.d.
Dt21	Single-stranded DNA	n.d.
SSDNA	Single-stranded DNA	0.055±0.007
CTDNA	Duplex-stranded DNA	0.032±0.005
Ds26	Duplex-stranded DNA	0.048±0.003
Bcl-2	G-quadruplex DNA	0.702±0.083
Ckit2	G-quadruplex DNA	0.923±0.028
RET	G-quadruplex DNA	0.743±0.019
VEGF	G-quadruplex DNA	0.705±0.080
Telo21	G-quadruplex DNA	1.161±0.125
Pu27	G-quadruplex DNA	1.146±0.165
tRNA	Transfer RNA	0.669±0.060
G4-RNA	G-quadruplex RNA	0.169±0.036
DsRNA	Duplex-stranded RNA	0.745±0.018
rRNA	Ribosomal RNA	3.009±0.268

[a] Equilibrium binding constant between the compound and nucleic acid at 25 °C;
n.d.: denotes not determined due to the ligand-substrates binding signal is too weak for estimation.

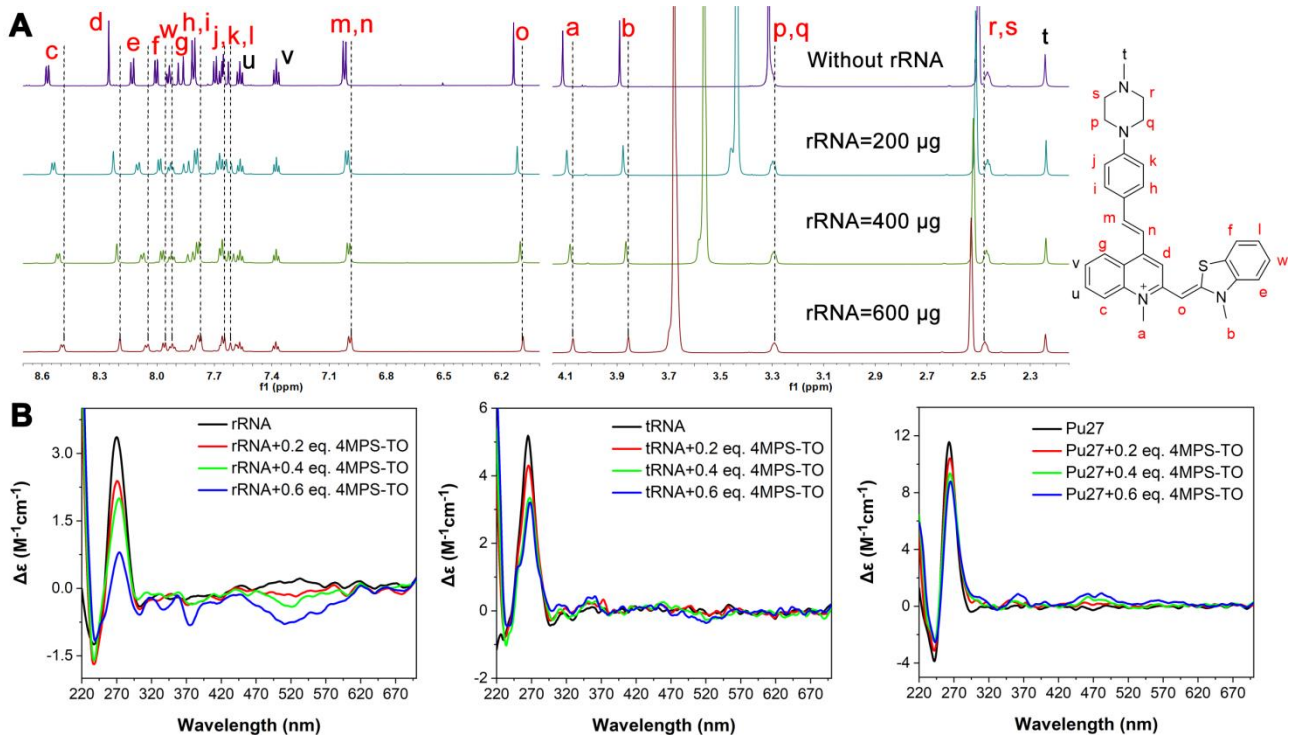

Figure 2. (A) ^{1}H NMR titration experiments of **4MPS-TO** (4 mg, DMSO-d_6) with rRNA (0-600 μg, D_2O-d_2). The experimental temperature was 25 °C. (B) CD spectra of rRNA (100 μg/mL), tRNA (100 μg/mL) or Pu27 G4-DNA (100 μg/mL) binding with ligand **4MPS-TO** (100 μg/mL) at pH 7.4 in a Tris-HCl buffer (10 mM, containing 60 mM KCl).

The equilibrium binding constants (K_{eq}) of **4MPS-TO** interacting with different substrates in a pH 7.4 buffer were determined (Table 1 and Figure S5). The results show that **4MPS-TO** has the highest affinity towards rRNA (K_{eq} = 3×10^5 M^{-1}), which is at least 3-4 folds higher than other substrates tested. The limit of detection (LOD) determined is 0.433 μg/mL (R^2 =0.9933, Figure 1C). Taken together, these results support that **4MPS-TO** is a selective and sensitive red fluorescent probe targeting rRNA under physiological conditions.

To further validate **4MPS-TO** interacted with rRNA in solution, we assigned the proton signals of the ligand by 2D ^{1}H NMR (Figure S6) and then NMR titration studies with rRNA at different concentrations were conducted (Figure 2A). The results showed that the proton signals labeled as *a, c, d, g* on the

quinoline moiety and *b, e, f, l, o, z* on the benzothiazole moiety of the ligand markedly decreased and shifted to the higher field as increasing the rRNA concentration in the titration. These results suggest that π-π stacking may occur on both quinoline and benzothiazole scaffolds with rRNA. For the (4-methylpiperazin-1-yl)styryl moiety, the *m, n, i, h, j, k* protons on the planar styryl group and the *p, q, r, s* protons on the flexible piperazinyl ring exhibit a clear chemical shift to high field, suggesting that these groups may also involve in the rRNA interaction.

In addition, circular dichroism (CD) spectroscopy was conducted to study the interaction of the ligand with rRNA in buffer. As shown in Figure 2B, the characteristic CD spectra of rRNA showed two distinct peaks at 240 nm (negative) and 270 nm (positive), respectively. When increasing the concentration of **4MPS-TO**, an obvious shift and loss of ellipticity of the characteristic CD peaks of rRNA are observed. Also, the induced CD signals with peaks located at 370 nm and 520 nm were markedly observed, indicating that **4MPS-TO**-rRNA interactions caused some degrees of conformational change of the rRNA. In contrast, for both tRNA and Pu27 G4-DNA, the ligand does not induce such obvious changes in the CD spectra. These results further suggest that the interaction of **4MPS-TO** with rRNA is stronger than that of tRNA and G4-DNA.

Intracellular Colocalization Imaging Studies. We then studied the performance of **4MPS-TO** in live cell imaging. For the HeLa cells treated with the ligand at 2.5 μM, red fluorescent signals were observed in both cytoplasmic and intranuclear regions (Figure 3A) and the rRNA-rich nucleolus region gave the most intensive red emission. The colocalization study with two known rRNA probes (E36 (Pearson correlation coefficient, Pr = 0.79) and Styryl-TO (Pr = 0.82), the green staining observed in Figure 3B) indicates that all these probes are well-colocalized in the cells. They probably bind to the same or similar

cellular targets. We also found that SYTO RNA-Select was not nuclear membrane permeable because no clear RNA-staining signal was found in nucleus (Figure S7).

The distribution of **4MPS-TO** in cytoplasm of live HeLa cells was investigated. The colocalization study of **4MPS-TO** with different organelle-specific dyes (Figure 3C and Figure S8) was performed. We found that **4MPS-TO** in the cytoplasmic region had a high overlapping (Pr = 0.53) with Mito-Green (a commercial mitochondrial targeting dye) and a low colocalization with the Golgi-Green (a commercial golgi apparatus targeting dye, Pr = 0.21) and Lyso-Green (a commercial lysosome targeting dye, Pr = 0.01). The results suggest that **4MPS-TO** most likely also binds to rRNAs in mitochondria of the cell.

To confirm the cellular substrate interacted with **4MPS-TO** is RNA but not DNA, enzymatic assays were performed (Figure 3D). For the HeLa cells treated with **4MPS-TO** and then were digested with DNase I, the red fluorescent signal of **4MPS-TO** remains essentially unchanged, indicating that the **4MPS-TO**-bound substrates in cells are not DNA. However, when the cells were treated with RNase A, the red fluorescent signal almost disappeared. The results confirm that the ligand is primarily bound to RNA in live cells. Furthermore, in fluorescence lifetime imaging (FLIM) experiments (Figure 3E), the number of photons collected at τ2 (1.31 ns) was peaked in the HeLa cells being incubated with **4MPS-TO**, while much fewer photons were collected at τ1 (0.38 ns) and τ3 (3.04 ns). The FLIM results suggest that the ligand may have a specific intracellular imaging target,[31] and presumably is rRNA. We also did fluorescence lifetime measurements for **4MPS-TO**-rRNA complex in buffer and the lifetime obtained was about 1.79 ns (Figure S9) that was comparable to the majority of photons collected at τ2 (1.31 ns) in live HeLa cells.[32] Therefore, the cellular target of **4MPS-TO** is suggested to be rRNA.

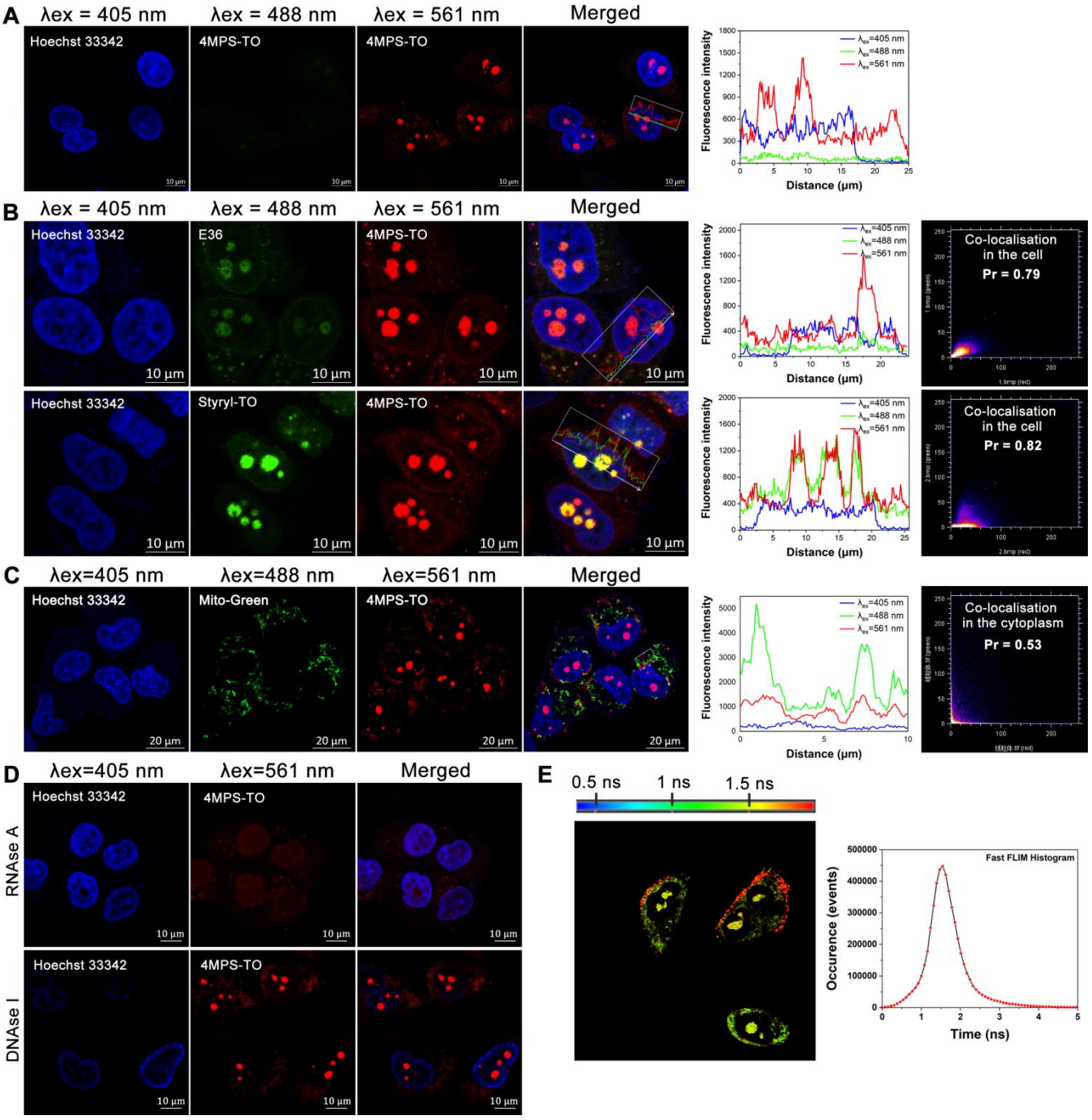

Figure 3. (A) Fluorescence images of live HeLa cells stained with **4MPS-TO** (2.5 μM) and nuclei stained with Hoechst 33342 (1.0 μM). (B) Fluorescence images of live HeLa cells stained with **4MPS-TO** (2.5 μM), RNA probe E36 (2.5 μM) or Stryl-TO (2.5 μM) and Hoechst 33342 (1.0 μM). (C) Fluorescence imaging images of co-localisation of **4MPS-TO** (2.5 μM) with Mito-Green (1 μM) dyes in HeLa cells. (D) Fluorescence imaging images of HeLa cells after **4MPS-TO** (2.5 μM) treatment with DNAse I or RNAse A. (E) FLIM images of HeLa cells incubated with **4MPS-TO** (2.5 μM) and the Lifetime Histogram displays the total number of counted photons over the lifetime (time difference after the laser pulse in nanoseconds).

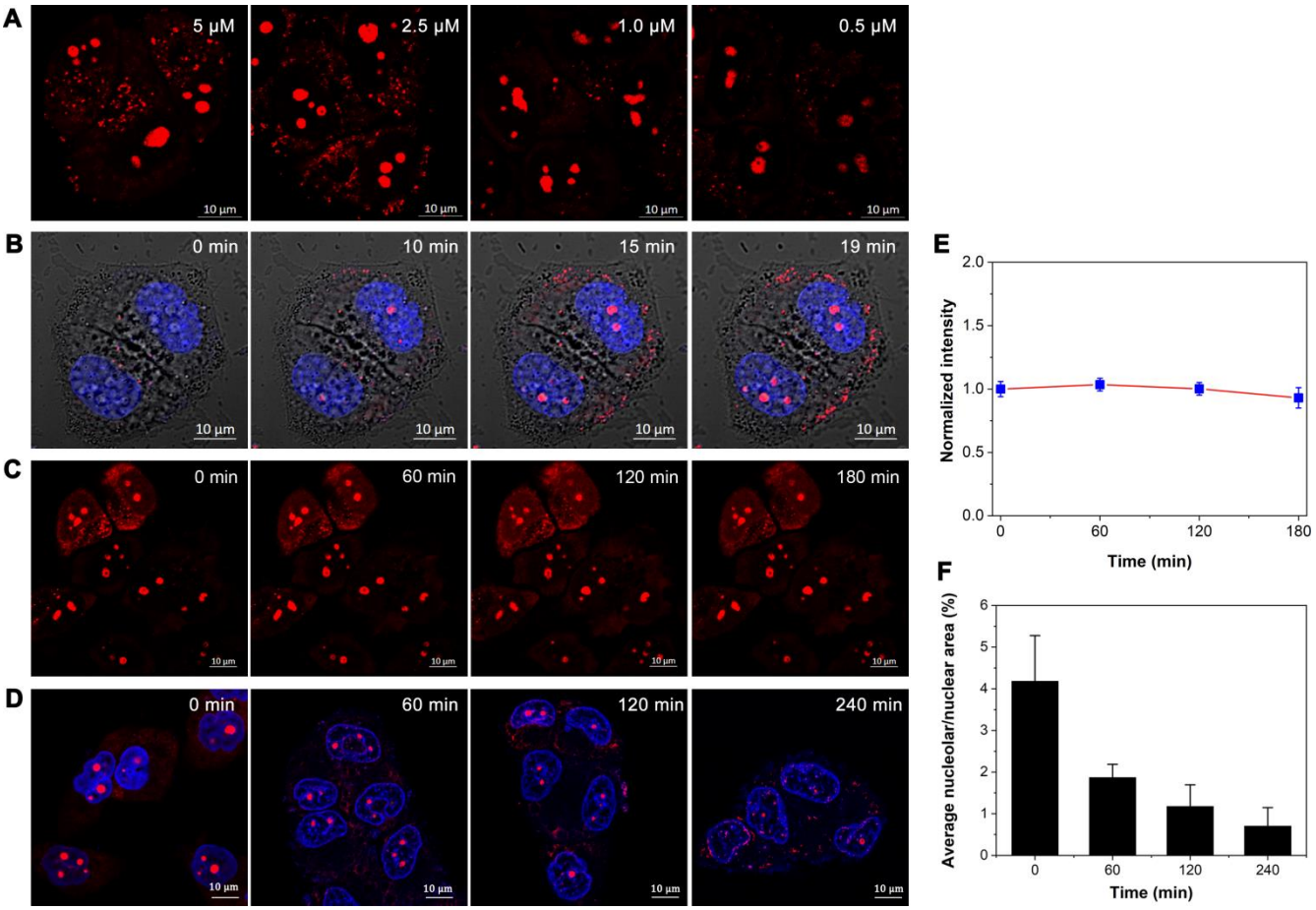

Figure 4. (A) Fluorescence images of live HeLa cells stained with different concentrations of **4MPS-TO** (0.5–5 μM). (B) Fluorescence images of live HeLa cells stained with **4MPS-TO** (1 μM) after 19 min. (C) Photobleaching ability assay of **4MPS-TO** (1 μM) in live HeLa cells (0–180 min). (D) Changes in nucleolus size were monitored. The HeLa cells after treated with actinomycin D (10 μg/mL) for 0–240 min and then stained with dyes (**4MPS-TO** (1 μM) and Hoechst 33342 (1 μM). (E) Photostability curve of **4MPS-TO** against photobleaching over a period of 0–180 min. (F) Quantification of mean nucleolus/nucleus area of HeLa cells after treatment with actinomycin D (10 μg/mL) for 0–240 min.

Intracellular Optical Properties and Toxicity Studies. Encouraged by the superior *in vitro* selectivity of **4MPS-TO** for rRNA sensing, we further investigated in detail for its performance to image rRNA in live cancer cells. The ligand at 0.5–5 μM was co-incubated and 1 μM Hoechst 33342 in live HeLa cells for 10 min for confocal imaging. As shown in Figure 4A, the red fluorescence signal was clearly visible in the cells even at 0.5 μM **4MPS-TO**. To evaluate its intracellular permeability, **4MPS-TO** at 1 μM was

used to track its internalization in live HeLa cells (Figure 4B). A clear red fluorescence was observed in both cytoplasmic and nucleolus regions of the HeLa cells at 10 min and the red fluorescent signal was saturated at about 20 min. Moreover, the ligand possesses better nuclear membrane permeability than the commercial probe SYTO RNA-Select in live cell imaging (Figure S7). The ligand also shows high photostability for at least 180 min in cells and buffer (Figure 4C,E and Figure S10), indicating that the probe allows long cellular experiments for monitoring or tracking of rRNA activity in live cells.

The cytotoxicity of the ligand was evaluated with a number of human cells. The MTT results (Figure S11 and Table S2) showed that, after incubation for 48 h, the IC_{50} of **4MPS-TO** was in the range of 5.5–9.2 μM for the cancer cell lines tested (HeLa, HepG2 and MCF-7) and was higher than 20 μM for the normal cell line (L-O2). It indicates that using **4MPS-TO** at low concentration (0.5–2.5 μM) for live cell imaging may cause no or low toxic effects on the normal physiological activity of the cells.

Monitoring the Change of Nucleolar Morphology. The investigation of **4MPS-TO** in real-time monitoring of nucleolus morphology was demonstrated in live cells. Actinomycin D is known a potent class of RNA synthesis inhibitor. It binds to the DNA template strand and then inhibits RNA synthesis to exert effects on the cellular nucleolus morphology.[33,34] As shown in Figure 4D and Figure 4F, HeLa cells were first treated with actinomycin D (10 μg/mL) for different time interval and then incubated with **4MPS-TO** for live cell imaging, a significant reduction in nucleolus area imaged with **4MPS-TO** (~75%) was observed with increasing the time for actinomycin D incubation from 0 to 240 min. This result not only suggests that the ligand can be used as a fluorescent probe to analyze the biological process involving the nucleolus, but also enables a rapid screening platform for potent RNA synthesis inhibitors like actinomycin D. Therefore, the ligand is a very useful fluorescent tool for chemical biology study and

drug development targeting rRNA.

One more live cell imaging demonstration is shown in Figure S12. When HeLa cells were treated with the rRNA synthesis inhibitor CX5461,[35,36] the red fluorescent signal of **4MPS-TO** at the nucleolus region was found almost disappeared. However, the red fluorescent signal of the **4MPS-TO**-treated HeLa cells was just slightly attenuated when the cells were treated with a G4-DNA stabilizer BRACO19.[37] These intracellular competition results further verify that **4MPS-TO** is rRNA-targeting in live HeLa cells and can be used for rapid screening rRNA inhibitors in drug discovery.

Dynamic Tracing of Mitochondrial Autophagy Process. In mitochondrial autophagy, lysosomes are known to act as scavengers to remove the damaged mitochondria to maintain an efficient cellular metabolism in cells. We thus induced oxidative stress in the mitochondria of live HeLa cells with H_2O_2,[38] and then monitored real-time the mitochondrial autophagy process with **4MPS-TO**. As shown in Figure 5, throughout a 90 min real-time monitoring of **4MPS-TO**-treated HeLa cells. From 0–20 min, the red foci (**4MPS-TO**) in the mitochondria were gradually approaching the green fluorescent spots (lysosomal probe), indicating that the lysosome was phagocytosing the mitochondria damaged by oxidative stress. Over time, 20–75 min, the lysosome (green foci) eliminated most of the damaged mitochondria (red foci) and more yellow fluorescent spots (merge of red and green foci) were observed. Afterwards, fewer yellow foci were observed (90 min). To confirm the fluorescent signal changes observed not causing by photobleaching, we conducted control experiments without H_2O_2 (Figure S13) for comparison. The quantified the results for the colocalization of **4MPS-TO**, shown in Figure S14, support that the H_2O_2 treatment induces obvious effects than the control, indicating that the fluorescent signal change observed in Figure 5 is not due to photobleaching. These real-time monitoring experiments demonstrate that

4MPS-TO can be utilized to track the physiological coordination of mitochondria and lysosomes during mitochondrial autophagy by targeting rRNAs localized in mitochondria.

A comparison of live cell imaging performance of 4MPS-TO with reported rRNA probes. In the present study, we found that **4MPS-TO** showed distinctive advantages over other reported probes (Table 2). Firstly, its emission wavelength is in the deep-red region that can reduce interference from background autofluorescence. Secondly, **4MPS-TO** has a high equilibrium binding constant with rRNA, meaning that it binds to rRNA with high affinity, which improves the sensitivity and selectivity in live cell assays. In addition, **4MPS-TO** is robust and has high photostability against photobleaching in the cells for more than 180 min. It is able to maintain a continuous and stable fluorescence signal for prolonged imaging experiments. More importantly, **4MPS-TO** also exhibits fast cell permeability. It enters the nucleus of live HeLa cells within 10 min for rapid imaging and real-time monitoring. Finally, **4MPS-TO** shows low cytotoxicity in the common human cell lines tested and has good biocompatibility. Collectively, our results support that the new rRNA-specific probe, **4MPS-TO**, is an excellent chemical tool for RNA sensing, live cell imaging, and rapid screening of rRNA inhibitors in drug discovery.

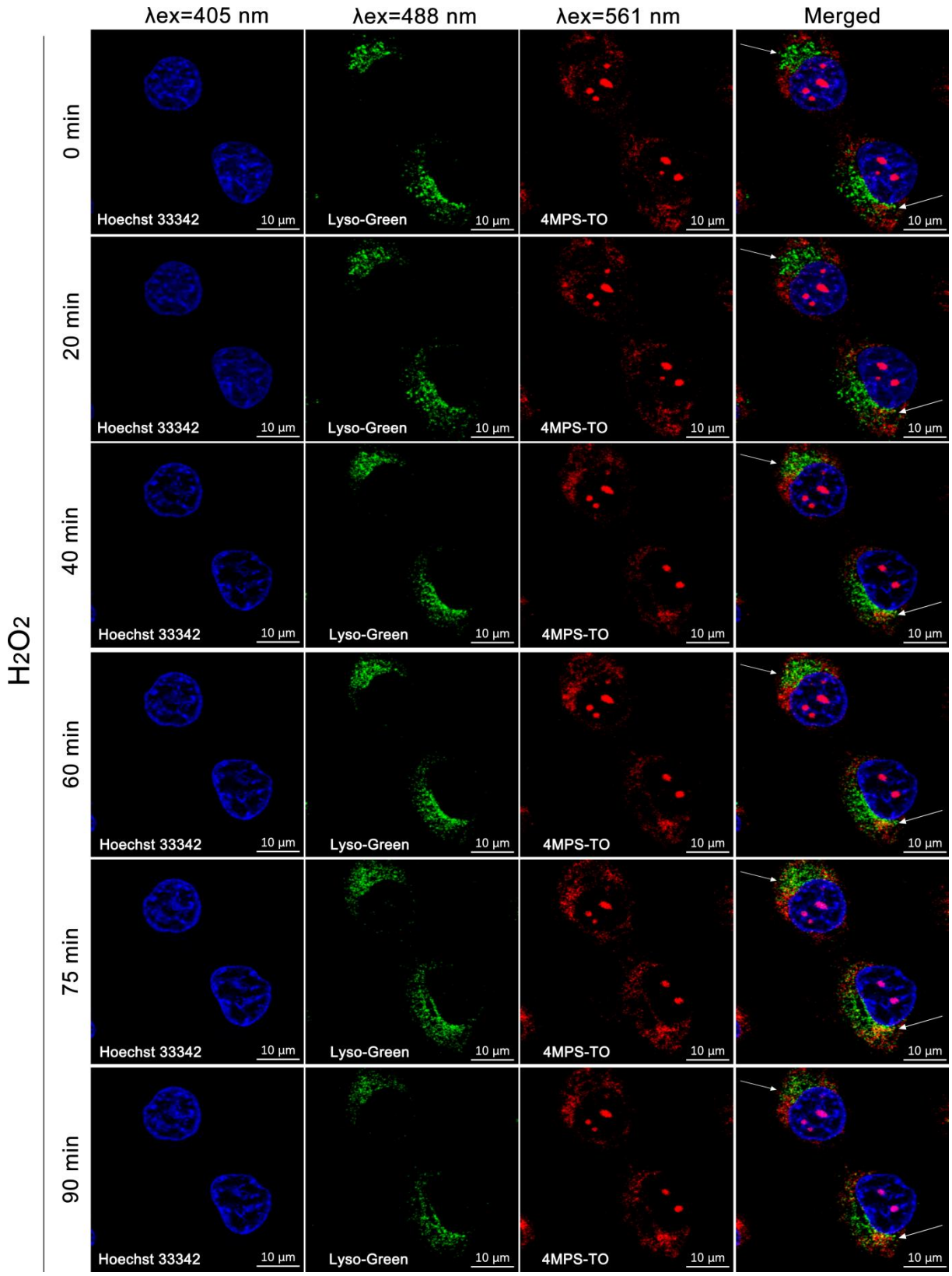

Figure 5. Live HeLa cells were incubated with Lyso-Green (1 μM), Hoechst 33342 (1 μM) and **4MPS-TO** (1 μM) for 30 min and then H_2O_2 (20 μM) was added, and fluorescence signals of each channel were collected from 0–90 min to observe the metabolic process of lysosome elimination of damaged

mitochondria during mitochondrial autophagy.

Table 2. Spectroscopic property, binding constant and cytotoxicity of recently reported RNA-targeting fluorescent probes.

rRNA probes	λ_{ex} /λ_{em} (nm)	K_{eq} [a] ($\times 10^5$ M^{-1})	Photo-stability [b]	Permeability time [c]	Cytotoxicity [d]
E36 [20,24]	497 / 548	0.89	< 15 min	25 min	3T3 cell 20 μM, > 70% (24 h)
Alkynylplatinum (II) derivative 1 [21]	550 / 670	0.60	–	60 min	HeLa cell 40 μM, > 90% (24 h)
Naphthalimide derivative 1 [22]	444 / 545	–	> 150 min	5 min	HeLa cell 30 μM, > 90% (6 h)
CP [23]	598 / 658	–	> 10 min	20 min	HeLa cell 10 μM, > 90% (24 h)
Styryl-TO [17]	476 / 535	12.32	> 180 min	15 min	–
PI2 [24]	409 / 511	4.48	> 15 min	20 min	3T3 cell 20 μM, > 90% (12 h)
4MPS-TO	520 / 620	3.01	> 180 min	10 min	HeLa, HepG2, MCF-7 cells IC_{50} = 5.5–9.2 μM (48 h)

[a] Equilibrium binding constant (K_{eq}) between the probes and rRNA.

[b] Photostability of the probe within cells.

[c] Time required for the probe to enter the nucleus.

[d] Cell viability (%) of the cells incubated with the compound.

CONCLUTIONS

In conclusion, a new red fluorescent probe selectively targeting rRNA was developed for molecule recognition and cell imaging in live human cancer cells. The probe exhibited strong photostability, high nuclear membrane permeability and biocompatibility in the cellular assays and showed better imaging performance than commercial rRNA probes. We also demonstrate that the probe can be utilized for real-time monitoring nucleolus morphology and mitochondrial autophagy targeting rRNA in live cancer cells. The probe may provide a useful, sensitive and target-specific fluorescent tool for chemical biology and drug discovery.

ASSOCIATEDCONTENT

Supporting Information

The Supporting Information is available free of charge at

Experimental methods and bioassay conditions (PDF).

Notes

The authors declare no competing interests.

Author Information

Corresponding Author

Wei Long - *State Key Laboratory of Chemical Biology and Drug Discovery, Department of Applied Biology and Chemical Technology, The Hong Kong Polytechnic University, Hung Hom, Kowloon, Hong*

Kong SAR 999077, China; The Hong Kong Polytechnic University Shenzhen Research Institute, Shenzhen 518057, P. R. China; ORCID: https://orcid.org/0000-0003-4739-2008; Email: wei-abct.long@polyu.edu.hk

Yu-Jing Lu - *School of Biomedical and Pharmaceutical Sciences, Guangdong University of Technology, Guangzhou 510006, P. R. China;* ORCID: https://orcid.org/0000-0003-2494-843X; Email: luyj@gdut.edu.cn

Wing-Leung Wong - *State Key Laboratory of Chemical Biology and Drug Discovery, Department of Applied Biology and Chemical Technology, The Hong Kong Polytechnic University, Hung Hom, Kowloon, Hong Kong SAR 999077, China; The Hong Kong Polytechnic University Shenzhen Research Institute, Shenzhen 518057, P. R. China;* ORCID: https://orcid.org/0000-0001-7191-7578; Email: wing.leung.wong@polyu.edu.hk

Authors

Jun-Ren Luo - *School of Biomedical and Pharmaceutical Sciences, Guangdong University of Technology, Guangzhou 510006, P. R. China*

Ze-Xin Chen - *School of Biomedical and Pharmaceutical Sciences, Guangdong University of Technology, Guangzhou 510006, P. R. China*

Shi-Min Wang - *School of Biomedical and Pharmaceutical Sciences, Guangdong University of Technology, Guangzhou 510006, P. R. China*

Yao-Xun Zeng - *The Hong Kong Polytechnic University Shenzhen Research Institute, Shenzhen 518057, P. R. China*

Bo-Xin Zheng - *State Key Laboratory of Chemical Biology and Drug Discovery, Department of Applied*

Biology and Chemical Technology, The Hong Kong Polytechnic University, Hung Hom, Kowloon, Hong Kong SAR 999077, China

Meng-Ting She - *The Hong Kong Polytechnic University Shenzhen Research Institute, Shenzhen 518057, P. R. China*

Author Contributions

All authors contributed significantly to the present study.

ACKNOWLEDGMENTS

The work described in this paper was substantially supported by the grant from the Research Grants Council of the Hong Kong Special Administrative Region, China (RGC Project No. 15300522), PolyU Departmental General Research Fund (P0045658), and National Natural Science Foundation of China (22077020). W.L. acknowledges the award of a postdoctoral fellowship administered by the Research Committee of The Hong Kong Polytechnic University. The University Research Facilities on Life Sciences and Chemical and Environmental Analysis of The Hong Kong Polytechnic University are acknowledged.

REFERENCES

(1) North, G. Back to the rna world and beyond. *Nature* **1987**, *328* (6125), 18–19.

(2) Szathmáry, E. The origin of the genetic code: amino acids as cofactors in an RNA world. *Trends. Genet.* **1999,** *15* (6), 223–229.

(3) Hombach, S.; Kretz, M. Non-coding RNAs: Classification, Biology and Functioning. *Adv. Exp. Med. Biol.* **2016,** 937, 3–17.

(4) Erdmann, V. A.; Barciszewska, M. Z.; Hochberg, A.; de Groot, N.; Barciszewski, J. Regulatory RNAs. *Cell. Mol. Life Sci.* **2001,** *58* (7), 960–977.

(5) Sloan, K. E.; Warda, A. S.; Sharma, S.; Entian, K. D.; Lafontaine, D. L. J.; Bohnsack, M. T. Tuning the ribosome: The influence of rRNA modification on eukaryotic ribosome biogenesis and function. *RNA Biol.* **2017,** *14* (9), 1138–1152.

(6) Bastide, A.; David, A. Interaction of rRNA with mRNA and tRNA in Translating Mammalian Ribosome: Functional Implications in Health and Disease. *Biomolecules* **2018,** *8* (4), 100.

(7) Derenzini, M.; Trerè, D.; Pession, A.; Govoni, M.; Sirri, V.; Chieco, P. Nucleolar size indicates the rapidity of cell proliferation in cancer tissues. *J. Pathol.* **2000,** *191* (2), 181–186.

(8) Zink, D.; Fischer, A. H.; Nickerson, J. A. Nuclear structure in cancer cells. *Nat. Rev. Cancer* **2004,** *4* (9), 677–687.

(9) Lamond, A. I.; Earnshaw, W. C. Structure and function in the nucleus. *Science* **1998,** *280* (5363), 547–553.

(10) Ni, C. Y.; Buszczak, M. Ribosome biogenesis and function in development and disease. *Development* **2023,** *150* (5), dev201187.

(11) Hein, N.; Hannan, K. M.; George, A. J.; Sanij, E.; Hannan, R. D. The nucleolus: an emerging target for cancer therapy. *Trends Mol. Med.* **2013,** *19* (11), 643–654.

(12) Bywater, M. J.; Pearson, R. B.; McArthur, G. A.; Hannan, R. D. Dysregulation of the basal RNA polymerase transcription apparatus in cancer. *Nat. Rev. Cancer* **2013,** *13* (5), 299–314.

(13) Xuan, J. C.; Gitareja, K.; Brajanovski, N.; Sanij, E. Harnessing the Nucleolar DNA Damage Response in Cancer Therapy. *Genes* **2021,** *12* (8), 1156.

(14) Scala, F.; Brighenti, E.; Govoni, M.; Imbrogno, E.; Fornari, F.; Treré, D.; Montanaro, L.; Derenzini, M. Direct relationship between the level of p53 stabilization induced by rRNA synthesis-inhibiting drugs and the cell ribosome biogenesis rate. *Oncogene* **2016,** *35* (8), 977–989.

(15) Harold, C. M.; Buhagiar, A. F.; Cheng, Y.; Baserga, S. J. Ribosomal RNA Transcription Regulation in Breast Cancer. *Genes* **2021,** *12* (4), 502.

(16) Petrov, A. S.; Bernier, C. R.; Hershkovits, E.; Xue, Y. Z.; Waterbury, C. C.; Hsiao, C. L.; Stepanov, V. G.; Gaucher, E. A.; Grover, M. A.; Harvey, S. C.; Hud, N. V.; Wartell, R. M.; Fox, G. E.; Williams, L. D. Secondary structure and domain architecture of the 23S and 5S rRNAs. *Nucleic Acids Res.* **2013,** *41* (15), 7522–7535.

(17) Lu, Y. J.; Deng, Q.; Hu, D. P.; Wang, Z. Y.; Huang, B. H.; Du, Z. Y.; Fang, Y. X.; Wong, W. L.; Zhang, K.; Chow, C. F. A molecular fluorescent dye for specific staining and imaging of RNA in live cells: a novel ligand integration from classical thiazole orange and styryl compounds. *Chem. Commun.* **2015,** *51* (83), 15241–15244.

(18) Chan, K. H.; Wang, Y. K.; Zheng, B. X.; Long, W.; Feng, X. X.; Wong, W. L. RNA-Selective Small-Molecule Ligands: Recent Advances in Live-Cell Imaging and Drug Discovery. *ChemMedChem* **2023,** *18*, e202300271.

(19) Zheng, B. X.; Yu, J.; Long, W.; Chan, K. H.; Leung, A. S. L.; Wong, W. L. Structurally diverse G-quadruplexes as the noncanonical nucleic acid drug target for live cell imaging and antibacterial study. *Chem. Commun.* **2023,** *59* (11), 1415–1433.

(20) Li, Q.; Kim, Y.; Namm, J.; Kulkarni, A.; Rosania, G. R.; Ahn, Y. H.; Chang, Y. T. RNA-selective, live cell imaging probes for studying nuclear structure and function. *Chem. Biol.* **2006,** *13* (6), 615–623.

(21) Law, A. S. Y.; Lee, L. C. C.; Lo, K. K. W.; Yam, V. W. W. Aggregation and Supramolecular Self-Assembly of Low-Energy Red Luminescent Alkynylplatinum(II) Complexes for RNA Detection, Nucleolus Imaging, and RNA Synthesis Inhibitor Screening. *J. Am. Chem. Soc.* **2021,** *143* (14), 5396–5405.

(22) Cao, C. Y.; Wei, P.; Li, R. H.; Zhong, Y. P.; Li, X.; Xue, F. F.; Shi, Y. B.; Yi, T. Ribosomal RNA-Selective Light-Up Fluorescent Probe for Rapidly Imaging the Nucleolus in Live Cells. *ACS Sensors* **2019,** *4* (5), 1409–1416.

(23) Zhou, B. J.; Liu, W. M.; Zhang, H. Y.; Wu, J. S.; Liu, S.; Xu, H. T.; Wang, P. F. Imaging of nucleolar RNA in living cells using a highly photostable deep-red fluorescent probe. *Biosens. Bioelectron.* **2015,** *68*, 189–196.

(24) Wang, C.; Lu, Y. J.; Cai, S. Y.; Long, W.; Zheng, Y. Y.; Lin, J. W.; Yan, Y.; Huang, X. H.; Wong, W. L.; Zhang, K.; Chow, C. F. Advancing small ligands targeting RNA for better binding affinity and specificity: A study of structural influence through molecular design approach. *Sensor. Actuat. B-Chem.* **2018,** *262*, 386–394.

(25) Suss, O.; Motiei, L. David, Broad Applications of Thiazole Orange in Fluorescent Sensing of Biomolecules and Ions. *Molecules* **2021,** *26* (9), 2828.

(26) Rye, H. S.; Yue, S.; Wemmer, D. E.; Quesada, M. A.; Haugland, R. P.; Mathies, R. A.; Glazer, A. N. Stable fluorescent complexes of double-stranded dna with bis-intercalating asymmetric cyanine dyes

- properties and applications. *Nucleic Acids Res.* **1992,** *20* (11), 2803–2812.

(27) Rye, H. S.; Glazer, A. N. Interaction of dimeric intercalating dyes with single-stranded-dna. *Nucleic Acids Res.* **1995,** *23* (7), 1215–1222.

(28) Long, W.; Zheng, B. X.; Huang, X. H.; She, M. T.; Liu, A. L.; Zhang, K.; Wong, W. L.; Lu, Y. J. Molecular Recognition and Imaging of Human Telomeric G-Quadruplex DNA in Live Cells: A Systematic Advancement of Thiazole Orange Scaffold To Enhance Binding Specificity and Inhibition of Gene Expression. *J. Med. Chem.* **2021,** *64* (4), 2125–2138.

(29) Jin, M.; Li, J.; Chen, Y.; Zhao, J.; Zhang, J. H.; Zhang, Z.; Du, P. Y.; Zhang, L. B.; Lu, X. Q. Near-Infrared Small Molecule as a Specific Fluorescent Probe for Ultrasensitive Recognition of Antiparallel Human Telomere G-Quadruplexes. *ACS Appl. Mater. Interfaces* **2021,** *13* (28), 32743–32752.

(30) Essam, Z. M.; Ozmen, G. E.; Setiawan, D.; Hamid, R. R.; Abd El-Aal, R. M.; Aneja, R.; Hamelberg, D.; Henary, M. Donor acceptor fluorophores: synthesis, optical properties, TD-DFT and cytotoxicity studies. *Org. Biomol. Chem.* **2021,** *19* (8), 1835–1846.

(31) Liu, L. Y.; Liu, W. T.; Wang, K. N.; Zhu, B. C.; Xia, X. Y.; Ji, L. N.; Mao, Z. W. Quantitative Detection of G-Quadruplex DNA in Live Cells Based on Photon Counts and Complex Structure Discrimination. *Angew. Chem., Int. Ed.* **2020,** *59* (24), 9719–9726.

(32) Berezin, M. Y.; Achilefu, S. Fluorescence Lifetime Measurements and Biological Imaging. *Chem. Rev.* **2010,** *110* (5), 2641–2684.

(33) Cortes, C. L.; Veiga, S. R.; Almacellas, E.; Hernández-Losa, J.; Ferreres, J. C.; Kozma, S. C.; Ambrosio, S.; Thomas, G.; Tauler, A. Effect of low doses of actinomycin D on neuroblastoma cell

lines. *Mol. Cancer* **2016,** *15*, 1.

(34) Yung, B. Y. M.; Chang, F. J.; Bor, A. M. S. Modulation of the reversibility of actinomycin-D cytotoxicity in HeLa-cells by verapamil. *Cancer Lett.* **1991,** *60* (3), 221–227.

(35) Drygin, D.; Lin, A.; Bliesath, J.; Ho, C. B.; O'Brien, S. E.; Proffitt, C.; Omori, M.; Haddach, M.; Schwaebe, M. K.; Siddiqui-Jain, A.; Streiner, N.; Quin, J. E.; Sanij, E.; Bywater, M. J.; Hannan, R. D.; Ryckman, D.; Anderes, K.; Rice, W. G. Targeting RNA Polymerase I with an Oral Small Molecule CX-5461 Inhibits Ribosomal RNA Synthesis and Solid Tumor Growth. *Cancer Res.* **2011,** *71* (4), 1418–1430.

(36) Kang, C. W.; Hannan, K. M.; Blackburn, A. C.; Loh, A. H. P.; Hong, K. C.; Yuan, G. J.; Hein, N.; Drygin, D.; Hannan, R. D.; Coupland, L. A. The therapeutic potential of RNA Polymerase I transcription inhibitor, CX-5461, in uterine leiomyosarcoma. *Invest. New Drugs* **2022,** *40* (3), 529–536.

(37) Gowan, S. M.; Harrison, J. R.; Patterson, L.; Valenti, M.; Read, M. A.; Neidle, S.; Kelland, L. R. A G-quadruplex-interactive potent small-molecule inhibitor of telomerase exhibiting in vitro and in vivo antitumor activity. *Mol. Pharmacol.* **2002,** *61* (5), 1154–1162.

(38) Luo, Z.; Xu, X.; Sho, T.; Zhang, J.; Xu, W. N.; Yao, J. B.; Xu, J. X. ROS-induced autophagy regulates porcine trophectoderm cell apoptosis, proliferation, and differentiation. *Am. J. Physiol. Cell Physiol.* **2019,** *316* (2), C198–C209.

GRAPHICAL ABSTRACT